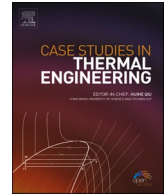




ELSEVIER

Contents lists available at ScienceDirect

## Case Studies in Thermal Engineering

journal homepage: [www.elsevier.com/locate/csite](http://www.elsevier.com/locate/csite)

# Performance enhancement mechanisms and optimization of multi-pass parallel flow condensers with liquid-vapor separation

Jin Huan Pu<sup>a</sup>, Nan Hua<sup>b,c,\*</sup>, Xiaodong Jian<sup>d</sup>, Ying Chen<sup>e</sup>, Yongliang Li<sup>f</sup>,  
Tong Yang<sup>g</sup>, Hua Sheng Wang<sup>c</sup>

<sup>a</sup> Institute for Advanced Technology, Shandong University, Jinan, Shandong, 250061, China

<sup>b</sup> Ningbo Institute of Technology, Beihang University, Ningbo, Zhejiang, 315832, China

<sup>c</sup> School of Engineering and Materials Science, Queen Mary University of London, London, E1 4NS, UK

<sup>d</sup> The Science and Technology on Reliability Physics and Application of Electronic Component Laboratory, The 5th Electronics Research Institute of the Ministry of Industry and Information Technology, Guangzhou, Guangdong, 510610, China

<sup>e</sup> School of Material and Energy, Guangdong University of Technology, Guangzhou, Guangdong, 510006, China

<sup>f</sup> School of Chemical Engineering, University of Birmingham, Birmingham, B15 2TT, UK

<sup>g</sup> Faculty of Science and Technology, Middlesex University, London, NW4 4BT, UK

## ARTICLE INFO

## Keywords:

Condenser  
Liquid-vapor separation  
Heat transfer  
Pressure drop  
Entropy generation  
Numerical simulation

## ABSTRACT

This study employed a distributed-parameter model developed by the authors to investigate the mechanisms of condensation heat transfer enhancement using liquid-vapor separation (LS) in multi-pass parallel flow condensers (MPFCs). Additionally, tube pass arrangements for MPFCs with LS were optimized. Simulations characterized relationships among refrigerant flow rate, vapor quality, flow patterns, heat-transfer coefficient and pressure drop at tube level, along with heat-transfer coefficient and tube-wall temperature distributions at the segment level. An entropy analysis based on the second law of thermodynamics quantified contributions from heat transfer and pressure drop. The results demonstrate that introducing LS leads to (1) a 9.1 % increase in the average heat-transfer coefficient, (2) a 50.4 % reduction in pressure drop, (3) similar entropy generation numbers due to heat transfer for both MPFC and MPFC-LS, (4) significantly higher entropy generation numbers due to pressure drop in the last two tube passes, and (5) a 51.4 % lower average entropy generation number for MPFC-LS compared to MPFC. Compared to a baseline serpentine condenser, MPFCs-LS reduced pressure drop by 84 %–98 % while maintaining nearly the same heat transfer rate, resulting in an overall performance improvement of 5 %–9 %. The optimal tube-pass arrangement for MPFCs-LS was identified as 3-3-2-2-2-2-1-1-1-1.

## 1. Introduction

Air-to-refrigerant condensers are important components for refrigerators, air conditioners and heat pumps. In recent decades, various heat transfer enhancement methods have been developed to improve their performance for more compact, higher efficiency and lower refrigerant inventory. Of these, considerable attention has been paid to passive enhancement techniques applied to the tube side due to no requirement of external power. Such as mini/microchannels [1–3], microfin tubes [4,5] and helical wire inserts [6,7].

Liquid-vapor separation technology, a newly developed innovation first introduced by Oh et al. [8] and Peng et al. [9], has been

\* Corresponding author. Ningbo Institute of Technology, Beihang University, Ningbo, Zhejiang, 315832, China.

E-mail address: [huanan@buaa.edu.cn](mailto:huanan@buaa.edu.cn) (N. Hua).

<https://doi.org/10.1016/j.csite.2025.106120>

Received 18 December 2024; Received in revised form 6 February 2025; Accepted 13 April 2025

Available online 15 April 2025

2214-157X/© 2025 The Authors. Published by Elsevier Ltd. This is an open access article under the CC BY-NC license (<http://creativecommons.org/licenses/by-nc/4.0/>).

## Nomenclature

$COP$	coefficient of performance
$d_i$	fin tip diameter of the tube
$D_o$	outside tube diameter
$G$	mass, $\text{kg m}^{-2} \text{s}^{-1}$
$h_f$	fin height
$HTC$	heat transfer coefficient, $\text{W m}^{-2} \text{K}^{-1}$
$i$	tube pass index
$j$	flow path index
$m$	mass flow rate, $\text{kg s}^{-1}$
$N_f$	number of the louvre fins along a tube
$N_s$	entropy generation number
$N_{mf}$	number of microfin
$P$	pressure, kPa
$P_l$	longitudinal tube pitch
$P_t$	transverse tube pitch
$\Delta P$	pressure difference, kPa
$Q$	heat transfer rate, W
$s$	entropy, $\text{J kg}^{-1} \text{K}^{-1}$
$S_{gen}$	entropy generation rate, $\text{W K}^{-1}$
$S_h$	height of a slit
$S_n$	number of slit in an enhanced zone
$S_s$	breadth of a slit in the direction of air flow
$T$	temperature, $^{\circ}\text{C}$
$t_b$	fin width at fin root
$\Delta T$	temperature difference, $^{\circ}\text{C}$

### Greek symbols

$\beta$	spiral/helix angle
$\gamma$	apex angle
$\rho$	density, $\text{kg m}^{-3}$
$\chi$	vapor quality
$\delta_f$	fin thickness

### Subscripts

a	air
ave	average
in	inlet
out	outlet
r	refrigerant
t	tube
w	tube-wall

### Acronyms

LS	liquid-vapor separation
MPFC	multi-pass parallel flow condenser
MPFC-LS	multi-pass parallel flow condenser with liquid-vapor separation

proposed and explored as a means to improve heat transfer coefficient and decrease pressure drop in multi-pass parallel flow condensers (MPFCs). This approach is designed to effectively remove condensate from the system through vapor-liquid separators during the phase transition from vapor to liquid. This leads to a thinner liquid film on the inner-tube surfaces. As a result, the increased heat transfer resistance caused by condensate accumulation on the walls during condensation is effectively minimized [10]. Fig. 1 illustrates the configurations of MPFCs and the novel liquid-vapor separation concepts. The two headers are equipped at both ends of parallel tubes and a number of bafflers are set in the headers, dividing the whole condenser into several tube-passes and consequently dividing the refrigerant flow inside the parallel tubes. The differences of these new concepts are shown based on their principles of liquid-vapor separation (Fig. 1(a) and (c)) and vapor bypass (Fig. 1(b)) in headers. Fig. 1(a) shows a multi-stage gas and liquid phase separation condenser proposed by Oh et al. [11]. The first tube-pass is located in the middle of the condenser while the vapor tube-passes and the liquid tube-passes are located in the upper and lower parts of the condenser, respectively. The outlet header is placed at the right-hand side of the condenser. When the two-phase refrigerant leaving from the first tube-pass enters into the center of

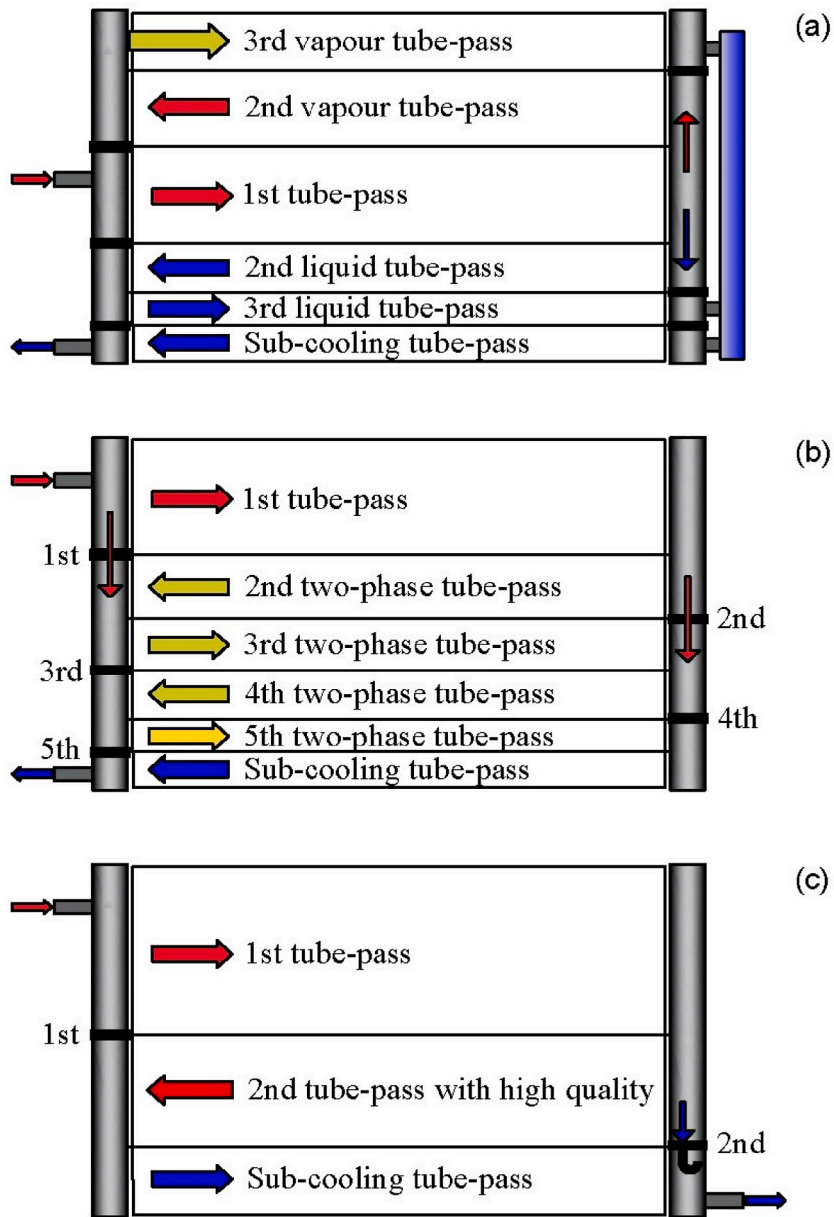


Fig. 1. Schematic illustrations of liquid-vapor separation methods: (a) Oh et al. [11], (b) Ye et al. [16] and (c) Jia et al. [17].

the outlet header, the vapor flows upward while the liquid flows downwards due to gravity force. Li and Hrnjak [12–15] further studied this type of liquid-vapor separation numerically and experimentally. Their visual observations suggested that better two-phase separation can be achieved by reducing the momentum upward of liquid and decreasing the interaction between liquid and vapor. Furthermore, the experimental results showed that when phase separation was implemented to the microchannel condenser of a R134a mobile air conditioning system, the coefficient of performance (COP) improvement raised by up to 6.6 % in comparison of the original system. Fig. 1(b) illustrates a two-phase zone enlargement technique proposed by Ye et al. [16]. As shown in Fig. 1(b), the first and second baffles have a pass-through hole each, which is treated as a distributor. When the superheated vapor flows into the inlet header of the first tube-pass, a small portion of refrigerant vapor directly leaps through the hole of the first baffle into the inlet header of the third tube-pass. The superheated vapor induces rigorous turbulence mixing when it injects into the header and merges with the mainstream from the second tube-pass. Similarly, some of the refrigerant goes through the hole of the second baffle and the turbulence mixing occurs in the inlet header of the fourth tube-pass. The essence of this technique is that introducing vapor bypass enlarges the two-phase flow zone of higher heat transfer and reduces the superheated zone of lower heat transfer in the condenser. Tests and flow visualizations were conducted to evaluate the performance of MPFCs with and without the distributors. Results indicated that the cooling performance of the MPFC with the distributors increased up to 9.6 % while its refrigerant mass flow increased by 13.3 %. As

depicted in Fig. 1 (c), a MPFC with a liquid-vapor separator beneath the second baffle at the right-hand side was developed by Jia [17]. This separator separates the condensate from the main stream, similar mechanism to the design shown in Fig. 1(a). A U-type liquid sealing tube serves as the liquid-vapor separator. When the wet vapor leaving the first tube-pass flows into the right header, the condensate accumulated at the bottom of header due to gravity, where part of the condensate is separated by the U-type liquid-vapor separator and as a result the refrigerant vapor quality entering the second tube-pass increases. The results of their experiments [18,19] showed that the heat-transfer coefficient of R134a was enhanced by 20 %–40 % in the second tube-pass and the of the overall heat-transfer coefficient was improved by 10 %–20 %, under conditions of saturation temperature 20 °C and mass flux in the range of 74 kg·m<sup>-2</sup> to 212 kg·m<sup>-2</sup>.

In this work, a MPFC incorporated with a continued liquid-vapor separation technology to facilitate condensation between adjacent tube-passes is investigated. Different from the liquid-separation concepts described above, the baffles in headers serve as liquid-vapor separators directly. These baffles have been purposely designed with nonuniform-diameter orifices of approximately 0.5 mm–2 mm 0.0 mm, as illustrated in Fig. 2. When two-phase refrigerant flows into the intermediate headers, the condensate accumulates on the top surface of the baffle forming a liquid film. This liquid film blocks the vapor flow but allows the condensate to pass through the orifices due to the capillary force and the pressure difference established between the two sides of the baffle. The two-phase refrigerant with increased vapor quality then has to flow into the next adjacent tube-pass. Wu et al. [20] and Chen et al. [21] conducted the replacement experiments in split-type domestic air conditioners. Compared with the MPFC without LS, the prototype condenser with liquid-vapor separation (MPFC-LS) showed 26.9 % reduction in heat-transfer area and 19.7 % reduction in refrigerant inventory.

This kind of MPFCs-LS has been extensively investigated at the component level of heat exchangers, including numerical simulations [22–24], visualization studies [25], and performance experiments [26,27]. Additionally, they have been explored at the system level in various applications such as vapor compression refrigeration [20,21,28–31], heat pumps [32–34] and organic Rankine cycles (ORC) [35–38]. The benefits of integrating LS into thermal systems have been well-documented. For instance, in air-conditioning systems [31], incorporating LS has led to a 9.8 % increase in EER during cooling mode and a 7.3 % increase in COP during heating mode compared to conventional systems. In heat pump systems [32], the inclusion of LS resulted in a 0.19 higher COP<sub>t</sub>, a 31.9 W reduction in time-average power consumption, a 30 g reduction in refrigerant charge, and a 4.88 % increase in efficiency, with almost equivalent time-averaged heat capacities. For ORCs [38], the thermal efficiency of with LS was found to be up to 64.8 % higher than that of an ORC using a serpentine condenser.

Despite these findings, there has been limited attention to the parametric analysis and comparison of local characteristics in condensers using LS, especially considering the maldistribution of mass flow rate within tubes. To better understand the mechanisms underlying the enhancement of condensation heat transfer induced by LS technology and to provide a more robust basis for the analysis, design and performance optimization of MPFCs-LS, a distributed-parameter model previously developed by the authors [23] was used. This work utilizes this model to predict and interpret the effects of liquid-vapor separation on both the local and overall performances of MPFCs, with a focus on flow maldistribution. Performance analyses comparing MPFCs with and without LS will be conducted based on the first and second laws of thermodynamics. Moreover, liquid-vapor separation condensation technology is recognized as an effective method for enhancing heat transfer during two-phase condensation inside the tubes. Given that air-side structural factors are assumed to have no significant impact, the design of MPFC-LS must carefully address the refrigerant side, particularly the liquid-vapor separation baffles, which must meet appropriate vapor-liquid separation efficiency requirements. Another critical aspect of the design involves optimizing the arrangement of tube passes, which is one of the most adjustable conditions of MPFC-LS design. Consequently, this work will finalize the optimization of the tube pass arrangement for the MPFC-LS, employing an overall efficiency metric that considers both heat transfer performance and pressure drop.

## 2. Numerical modelling

To clarify the mechanisms of condensation heat transfer enhancement using liquid-vapor separation technology in MPFCs, the numerical simulations and a comparison of thermal performance will be conducted using the MPFC-LS and MPFC models shown in

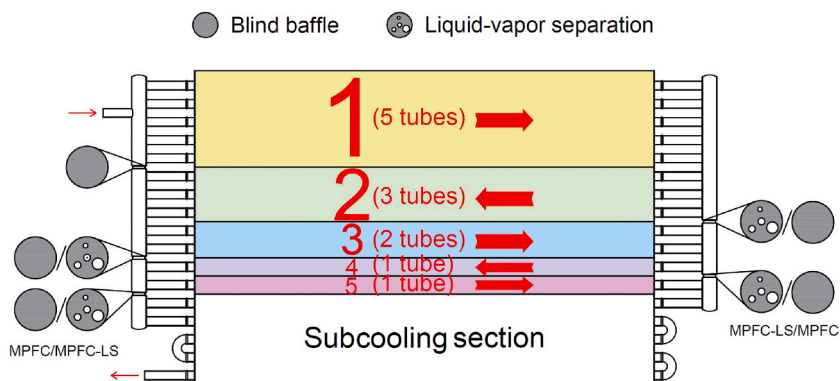


Fig. 2. Schematics of the condensers with and without LS.

Fig. 2. The geometric details, such as those for the fins, tubes and headers, can be found in Table 1. The other main configurations and working conditions are described below. As depicted in Fig. 2, the calculation domain of heat transfer is the color blocks in the schematics of the two condensers, containing a total of twelve heat-transfer tubes. These blocks denote the first five tube-passes marked and constitute a classic condenser with the subcooling section removed.  $5 \rightarrow 3 \rightarrow 2 \rightarrow 1 \rightarrow 1$  is the number distribution of tube-passes, where the numbers refer to the number of tubes in each tube-pass. For the MPFC-LS modelling, when the baffles serve as LS, the vapor quality of refrigerant flow is assumed as 1.0 at the entrance of the next tube-pass, i.e. the condensate obtained through the previous tube-pass is completely subtracted from the mainstream. The simulation conditions are listed in Table 2. R134a is used as the refrigerant in tubes. It should be noted that the frontal air flow for both MPFC-LS and MPFC is treated as uniform, and the air velocities are iterated to achieve the given heat transfer rate of 1300 W. The velocity ranged between 2.0 and 2.5 m/s.

A 2-D distributed-parameter model for MPFCs-LS, developed in the authors' earlier work [23,39], will be employed for the numerical investigation of the underlying mechanism and the optimization analysis of MPFCs-LS. The model operates on three levels: condenser level, tube-pass level and branch level. The condenser is divided into tube passes, separated by the baffles in the headers. Each tube pass comprises several branches, or tubes, connected to the headers at both ends. Each branch is further divided into three types of elements: dividing T-junction, combining T-junction and tube cells. The heat transfer tubes are segmented into finite control volumes along the direction of refrigerant flow, with each segment acting as a tube-centered element that represents an independent cross-flow interaction between the air flow outside and the refrigerant flow inside the tube. In the condenser, each tube pass is denoted by  $i$ , indicating its sequence along the refrigerant flow direction. The heat transfer tubes within a given tube pass are identified using  $i, j$ , where  $j$  specifies the tube's position within the  $i$ -th tube pass. Additionally, the tube is divided into discrete computational segments, labeled as  $i, j, k$ . Here,  $k$  represents the specific segment within the  $j$ -th tube of the  $i$ -th tube pass, corresponding to the current calculation position along the tube length.

To simplify the model, the following assumptions are applied: (1) The condenser operates under steady-state conditions; (2) Fins and headers are considered thermally insulated; (3) Axial heat conduction within the tubes is neglected; (4) The tube wall temperature is assumed to be uniform within each segment; (5) Thermodynamic properties of both refrigerant and air are uniform throughout each segment; (6) Both refrigerant and air flows are considered one-dimensional; (7) Air is assumed to flow straight through the heat exchanger; (8) The flow is assumed to be fully developed both thermally and hydraulically; (9) The refrigerant is considered fully mixed within the intermediate headers; (10) The flow distribution across each tube-pass section is assumed to be independent; (11) The inlet and outlet headers are modeled as a series of T-junctions for dividing and combining the flow, with no consideration for recirculation or flow perturbations between adjacent junctions.

Detailed information about this model can be found in Refs. [23,39]. For convenience, the key equations are provided in Table 3. The  $\epsilon$ -NTU, which does not require iteration solutions, was used to calculate heat transfer between the refrigerant and air sides. An algebraic method was employed to determine the refrigerant flow distribution. The correlations used in the present work for heat transfer and pressure drop are available in Tables 4 and 5.

The model accurately tracked the onset and completion of condensation within the refrigerant flow and determined flow maldistribution using a genetic algorithm. Flow patterns during condensation were identified to apply the appropriate correlations for heat transfer and pressure drop. The model showed strong agreement with experimental data [23], with root-mean-square deviations in heat transfer capacity and pressure drop within 7.5 % and 20.6 %, respectively.

### 3. Simulation results and discussion

#### 3.1. Analysis of average characteristics in tubes

The typical investigations [41,42] on condensation in microfin tube with the outer diameter of around 7.0 mm showed that the heat transfer and pressure drop mainly depend on the mass flux and vapor quality, as well as the flow pattern. Therefore, Figs. 3–5 demonstrate the comparison of mass flux  $G$ , averaged quality  $\chi_{ave}$ , flow pattern, averaged heat transfer coefficient  $HTC_{ave}$ , and pressure drop  $\Delta P$ , in tube-level of the condensers for MPFC-LS and MPFC without LS. The dash lines divide the figures into five zones sequentially, as the marks of tube-pass  $i$  as 1, 2, 3 and 4–5, which corresponds to the red number in Fig. 2. Moreover, since the first baffle for both condensers are blind, the simulation results in Tube-pass 1 of MPFC-LS and MPFC are overlapping in Figs. 3–5.

**Table 1**  
Geometrical parameters of the condensers [23].

Helical microfin tube	$D_o$ mm	$d_i$ mm	$p_t$ mm	$h_f$ mm	$t_b$ mm	$\beta$ deg	$\gamma$ deg	$N_{mf}$
	7.37	6.89	0.408	0.15	0.14	53	18	60
Slit-louvered fin	$F_s$ mm	$\delta_f$ mm	$P_l$ mm	$S_s$ mm	$S_h$ mm	$S_n$	$N_f$	$N_l$
	1.35	0.115	12.7	1.2	1.0	6	1	365

Note: outside tube diameter ( $D_o$ ); fin tip diameter of the tube ( $d_i$ ); transverse tube pitch ( $p_t$ ); fin height ( $h_f$ ); fin width at fin root ( $t_b$ ); spiral/helix angle ( $\beta$ ); apex angle ( $\gamma$ ); number of microfin ( $N_f$ ); fin pitch ( $F_s$ ); fin thickness ( $\delta_f$ ); longitudinal tube pitch ( $P_l$ ); breadth of a slit in the direction of air flow ( $S_s$ ); height of a slit ( $S_h$ ); number of slit in an enhanced zone ( $S_n$ ); number of longitudinal tube row ( $N_f$ ); number of the louvre fins along a tube ( $N_l$ ).

**Table 2**  
Simulation conditions of the condensers

Parameter	$m_{r,in}$ (kg s <sup>-1</sup> )	$P_{r,in}$ (kPa)	$\chi_{r,in}$	$T_{a,in}$ (°C)	Q (W)
Value	0.02	1160	0.95	35	1300

**Table 3**  
Summary of the key equations in the present work [23,39].

Type	Equation
Conservation of continuity, momentum and energy	Refrigerant side: $m_r(i, j, k) = m_r(i, j, k+1)$ $P_r(i, j, k) = P_r(i, j, k+1) + \Delta P_{fr}(i, j, k) + \Delta P_{m,r}(i, j, k)$ $m_r(i, j, k)h_r(i, j, k) = Q(i, j, k) + m_r(i, j, k+1)h_r(i, j, k+1)$ Air side: $m_a(i, j, k) = m_a(i, j, k)$ $P_{a,in}(i, j, k) = P_{a,out}(i, j, k) + \Delta P_{f,a}(i, j, k)$ $m_a(i, j, k)h_{a,in}(i, j, k) + Q(i, j, k) = m_a(i, j, k)h_{a,out}(i, j, k)$
Heat transfer: $\varepsilon$ -NTU	$Q(i, j, k) = \varepsilon(i, j, k)c_{min}(i, j, k)(T_r(i, j, k) - T_{a,in}(i, j, k))$ Single-flow in the segment: $\varepsilon(i, j, k) = 1 - \exp\left(-\frac{c_{max}(i, j, k)}{c_{min}(i, j, k)}\left(1 - \exp\left(-NTU(i, j, k)\frac{c_{min}(i, j, k)}{c_{max}(i, j, k)}\right)\right)\right)$ Condensing flow in the segment: $\varepsilon(i, j, k) = 1 - \exp(-NTU(i, j, k))$
Pressure drop	$\Delta P(i, j) = \Delta P_{inh}(i, j) + \Delta P_t(i, j) + \Delta P_{outh}(i, j)$ Note: inh (the inlet header part); t (the heat transfer tube part); outh (the outlet header part)
Refrigerant flow distribution	$\sum \Delta P[m(i, j-1)] = \sum \Delta P[m(i, j)]$ $\sum \Delta P = f[m(i, j-1)]$ $\sum \Delta P = f[m(i, j)]$

**Table 4**  
Summary of the correlations for heat transfer.

Fluid	Type	Source
Refrigerant side (two phase flow)	Heat transfer (annular flow regime)	Yu and Koyama [40] Cavallini et al. [41]
	Heat transfer (stratified-wave flow regime)	Kim et al. [42]
	Evaluation of the Annular flow and Stratified-wave flow regimes	Cavallini et al. [41]
Refrigerant side (single phase flow)	Heat transfer	Wu et al. [43]
Air side	Heat transfer	Wang et al. [44]

**Table 5**  
Summary of the correlations for pressure drop.

Fluid	Type	Source
Refrigerant side (two phase flow)	Frictional pressure drop (Annular flow regime)	Haraguchi et al. [45] Nozu et al. [46]
	Frictional pressure drop (Stratified-wave flow regime)	Kim et al. [42]
	Gravitational pressure drop	Collier and Thome [47]
	Contraction, and expansion loss	Collier and Thome [47]
Refrigerant side (single phase flow)	Frictional pressure drop	Thome [48]
	Gravitational pressure drop	Thome [48]
Refrigerant side of the headers	Minor loss due to tube protrusion	Yin et al. [49]
Air side	Pressure drop	Wang et al. [44]

3.1.1. Mass flux and averaged vapor quality in tubes

With the progress of condensation in tubes, void fraction is decreasing that results in the mean specific volume of the two-phase flow declines dramatically. Thus, in order to keep sufficient velocity inside tubes to avoid heat transfer deterioration, for MPFCs, the number of parallel tubes in tube-passes should be arranged by decreasing along the flow direction. As a result, the overall trend of the mass fluxes in tubes (red curves in Fig. 3) is going up for both the condensers along the flow direction. In addition, the total mass fluxes entering the tube passes ( $G(i) = \sum_{j=1}^N G(i, j)$ ) are decreasing in MPFC-LS, due to the condensate separated from the mainstream by liquid-vapor separation.  $j$  here refers to the tube number in tube-pass  $i$  in vertical direction. Consequently, the mass flux in tube-level of MPFC-LS is always lower than that of MPFC.

The averaged vapor quality of a tube,  $\chi_{ave}$ , as the blue lines shown in Fig. 3, is calculated by Eq. (1). Since the headers are treated as adiabatic in the present model,  $\chi_{in}$  and  $\chi_{out}$  here refer to vapor qualities at the inlet and outlet of the tube, respectively.

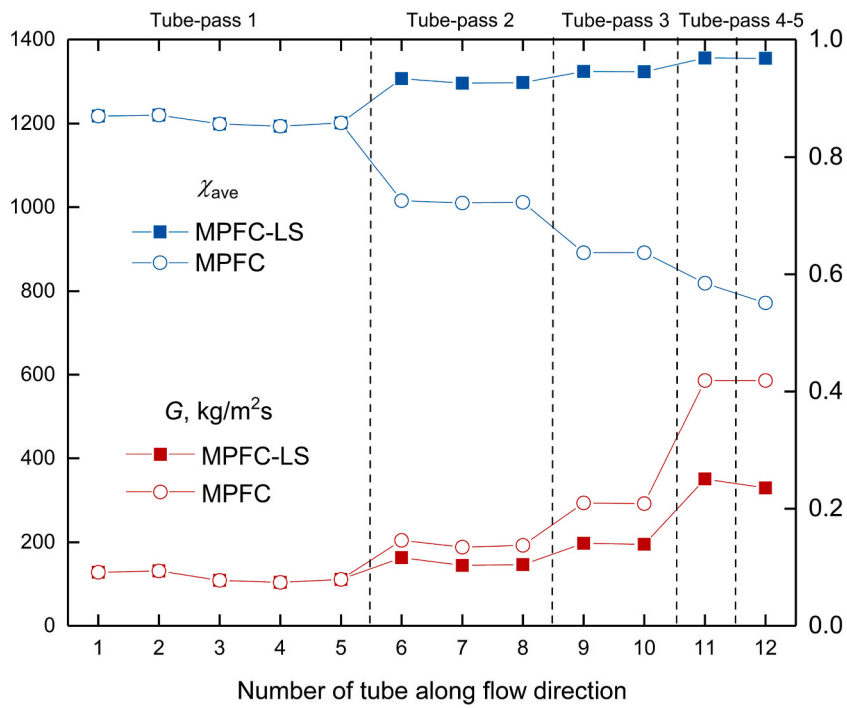


Fig. 3. Comparison of  $G$  and  $\chi_{ave}$  per tube for condensers with and without LS.

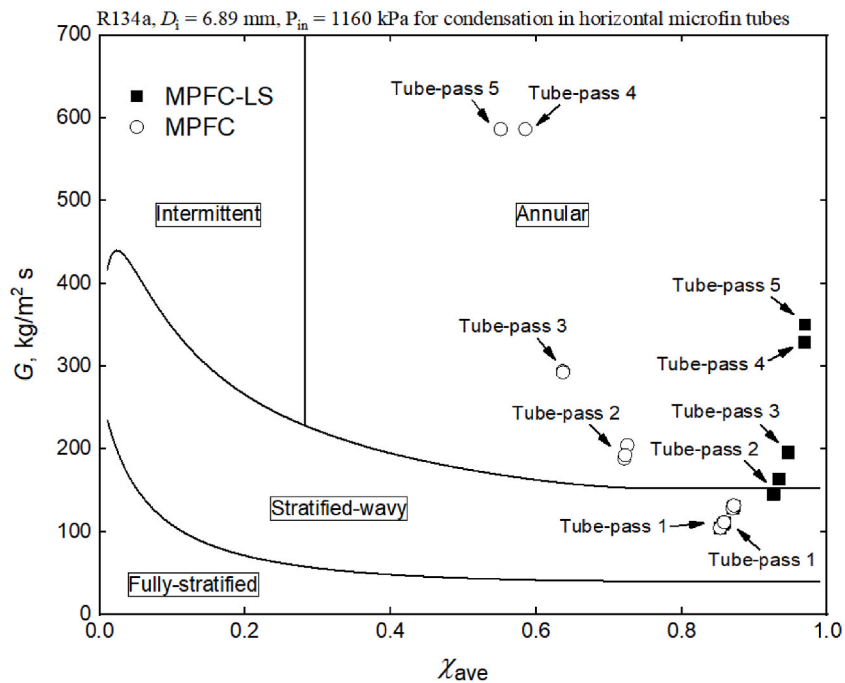


Fig. 4. Comparison of flow pattern in tubes for condensers with and without LS.

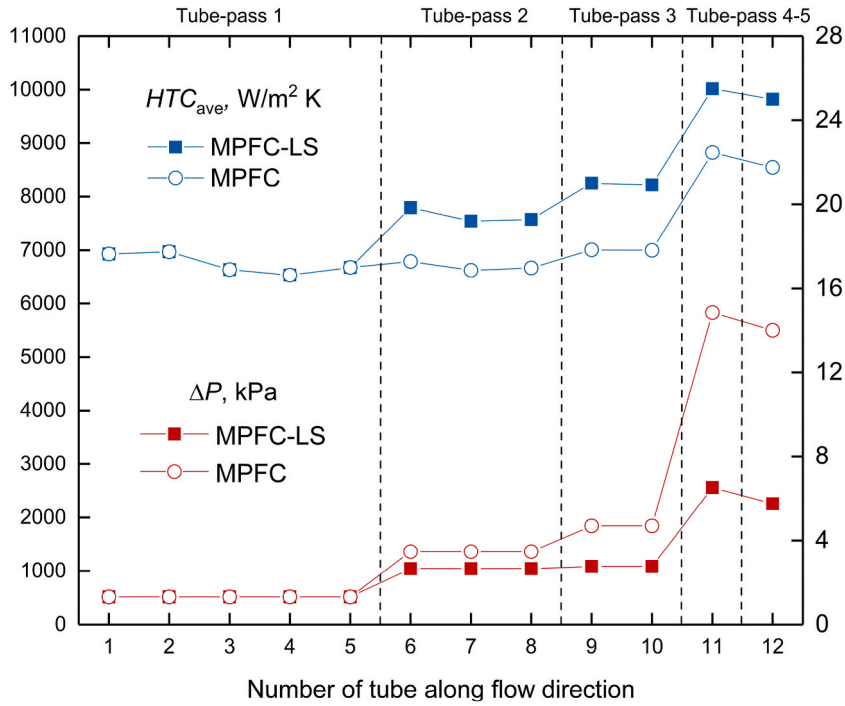


Fig. 5. Comparison of  $HTC_{ave}$  and  $\Delta P$  per tube for condensers with and without LS.

$$\chi_{ave}(i,j) = \frac{\chi_{in}(i,j) + \chi_{out}(i,j)}{2} \tag{1}$$

It can be found in the figure, for MPFC (blue hollow circles), the  $\chi_{ave}$  is decreasing along the whole condensation process, which is similar to that in a conventional condenser. In the MPFC-LS, however, the condensation is discontinuous. Prior to entering the next tube-pass, the two-phase refrigerant flow with relatively low vapor quality, which has just experienced the condensation in the previous tube-pass, drains the condensate in the media header through the liquid-vapor separator. Then condensate flows into the subcooling zone directly through the holes of baffles. Correspondingly, the vapor quality of the mainstream is evidently promoted. Thus, as depicted in Fig. 3, the MPFC-LS (blue solid squares) presents such a non-continuous feature that can maintain the averaged vapor quality in tubes at a very high level throughout the entire condenser, even beyond 0.9.

### 3.1.2. Estimation of flow pattern for refrigerant flow in tubes

As discussed in the authors' earlier work [23], in order to select the most appropriate empirical correlations to calculate heat transfer and pressure drop during condensation process, the flow regime that is expected to prevail in the tubes, should first be evaluated. Fig. 4 presents the flow patterns in tubes plotted on an existed flow map, which was proposed by Liebenberg and Meyer [50] for condensation in horizontal microfin tubes. For both of the MPFC-LS and MPFC, the two-phase refrigerant flows in Tube-passes 2–5 are in an annular flow regime, in which the higher mass flux and vapor quality lead to a higher heat transfer coefficient. The two-phase refrigerant flows in Tube-pass 1 for both condensers are all in the stratified-wave flow regime due to lower mass flux in these tubes.

### 3.1.3. Averaged heat transfer coefficient and pressure drop in tubes

The averaged heat-transfer coefficient,  $HTC_{ave}$ , in tubes as the blue lines shown in Fig. 5, is determined by Eq. (2), where  $M$  denotes the total number of segments taken for a heat-transfer tube and  $k$  denotes the number of the segment along the flow direction.

$$HTC_{ave}(i,j) = \frac{\sum_{k=1}^M HTC(i,j,k)}{M} \tag{2}$$

As seen in Fig. 5, under the comprehensive influence of mass flux and vapor quality, the averaged  $HTCs$  in Tube-passes 2–5 MPFC-LS are improved by 13.5%–17.8% than those of MPFC, though the averaged vapor qualities in the tubes of Tube-passes 4 and 5 have profound increases, even up to 75.6%. The results show that even without liquid-vapor separation the MPFC can still achieve a fair degree of heat transfer improvement at relatively low vapor quality (e.g.  $\chi_{ave}$  is 0.55) by keeping the high mass flux and high velocity in the tubes. Therefore, it is very important to optimize the number of tubes in a tube-pass, arrangement of tube-passes and liquid-vapor separation rate for the design of MPFCs-LS when the configurations and working conditions are given. The large number of parallel tubes in a tube-pass decreases the mass flow rate and hence the heat-transfer coefficient while the high liquid-vapor

separation rate in headers increases the vapor quality entering the parallel tubes and hence the heat-transfer coefficient.

As the red lines illustrated in Fig. 5, for both the MPFC-LS and MPFC, the overall trend of pressure drop in tube-level variation highly depends on the overall trend of mass flux in tubes in Fig. 3. Apparently, the mass flux here is the governing factor. For the two condensers, the two-phase annular flows occur in tubes of Tube-passes 2–5. With mass flux and vapor quality increasing, pressure gradient increases, which is due to the higher friction at higher vapor velocity (shear force dominated). For MPFC-LS, an appropriate number of tubes designed in tube-passes leads to the decreases of the pressure drop in tubes of Tube-passes 2–5, though the vapor quality increased by LS. The simulation results show the  $\Delta P$  in Tube-passes 2 and 3 of MPFC-LS are 23.4 % and 41.3 % lower than those of MPFC, respectively. These gaps are further enlarged in the downstream, which are 57.5 % and 58.9 % lower for Tube-passes 4 and 5, respectively.

3.2. Local distributions of heat-transfer coefficient and tube-wall temperature

In this section, the velocities and the temperatures at the inlet of air flow are assumed as uniform and constant, so the flow

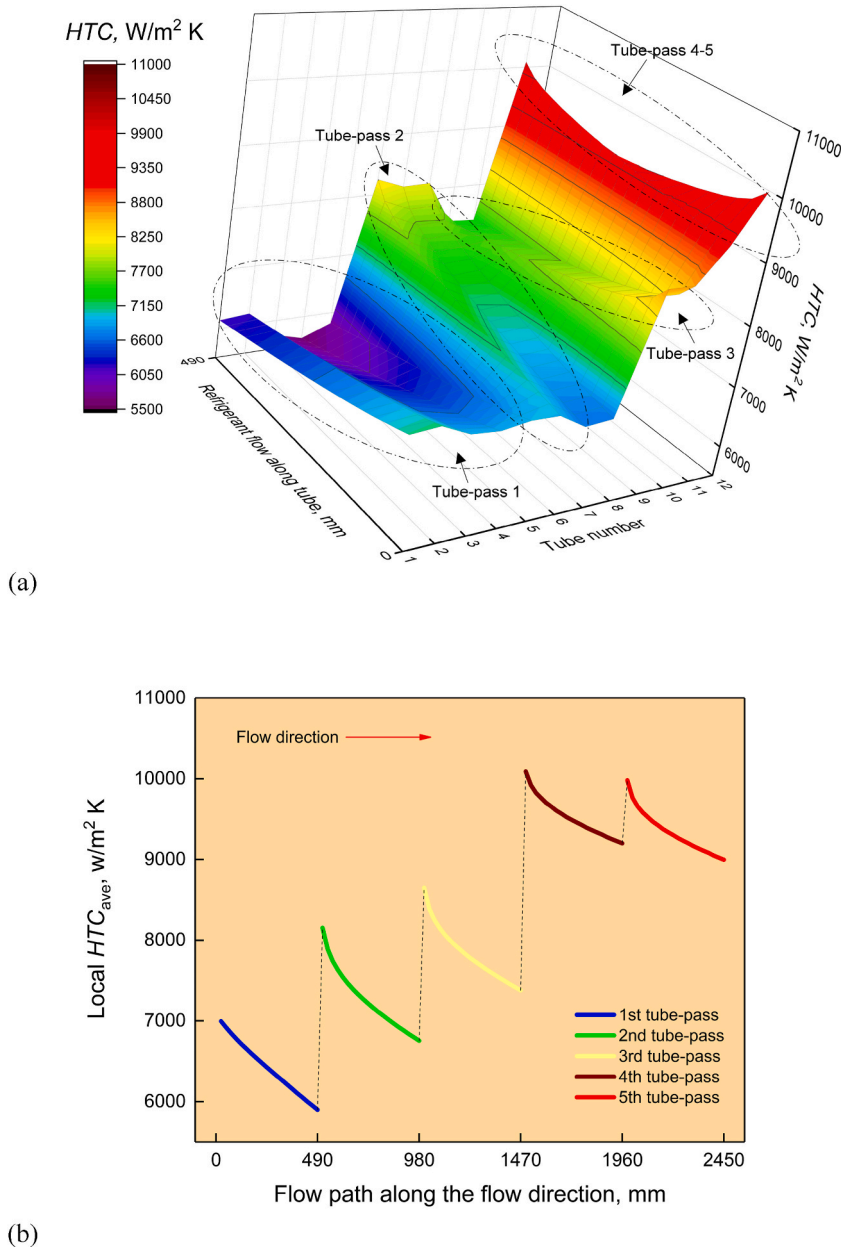


Fig. 6. (a) Local  $HTC$  of the MPFC-LS; (b) Local  $HTC_{ave}$  along tube-pass of the MPFC-LS.

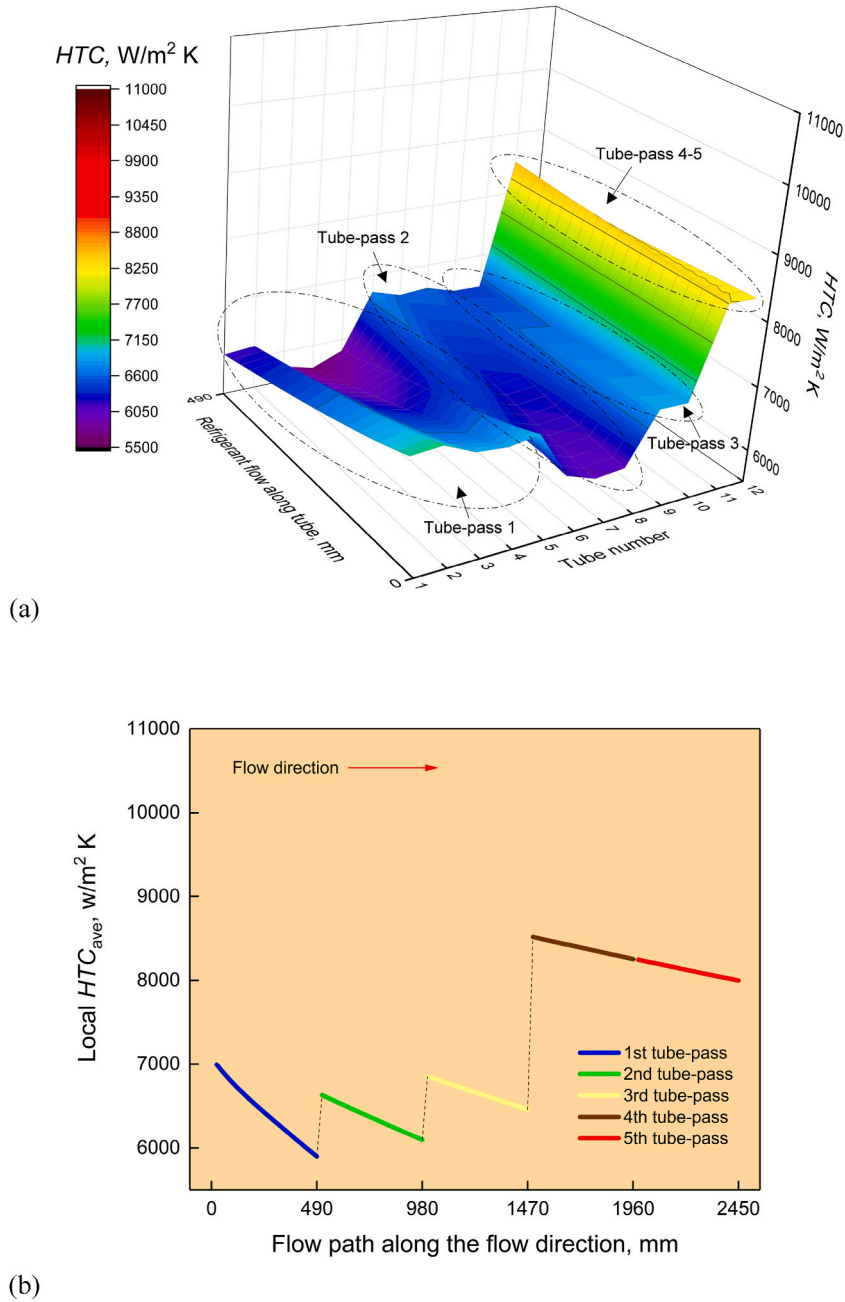


Fig. 7. (a) Local  $HTC$  of the MPFC; (b) Local  $HTC_{ave}$  along tube-pass of the MPFC.

maldistribution on the refrigerant side results in uneven heat transfer. Figs. 6–9 demonstrate the profiles of local  $HTC$  in refrigerant side and  $T_w$  facing the windward side of MPFC-LS and MPFC under the given conditions.

The distributions of local  $HTC$  by the views 3-D are described in Figs. 6(a) and 7(a). For convenience, the tubes and tube-pass arrangement of condensers in Figs. 6(a) and 7(a) should be interpreted along with Fig. 2. Figs. 6(b) and 7(b) are the local  $HTC_{ave}$  in tube-passes along the flow direction, which are determined by Eq. (3) as follows.

$$Local\ HTC_{ave}(i, k) = \frac{\sum_{j=1}^N HTC(i, j, k)}{N} \tag{3}$$

where  $N$  is the total number of parallel tubes in a tube-pass.

Compared the local  $HTCs$  in Fig. 6(a) to those in Fig. 7(a), Tube-passes 2–5 of MPFC-LS present significant heat transfer

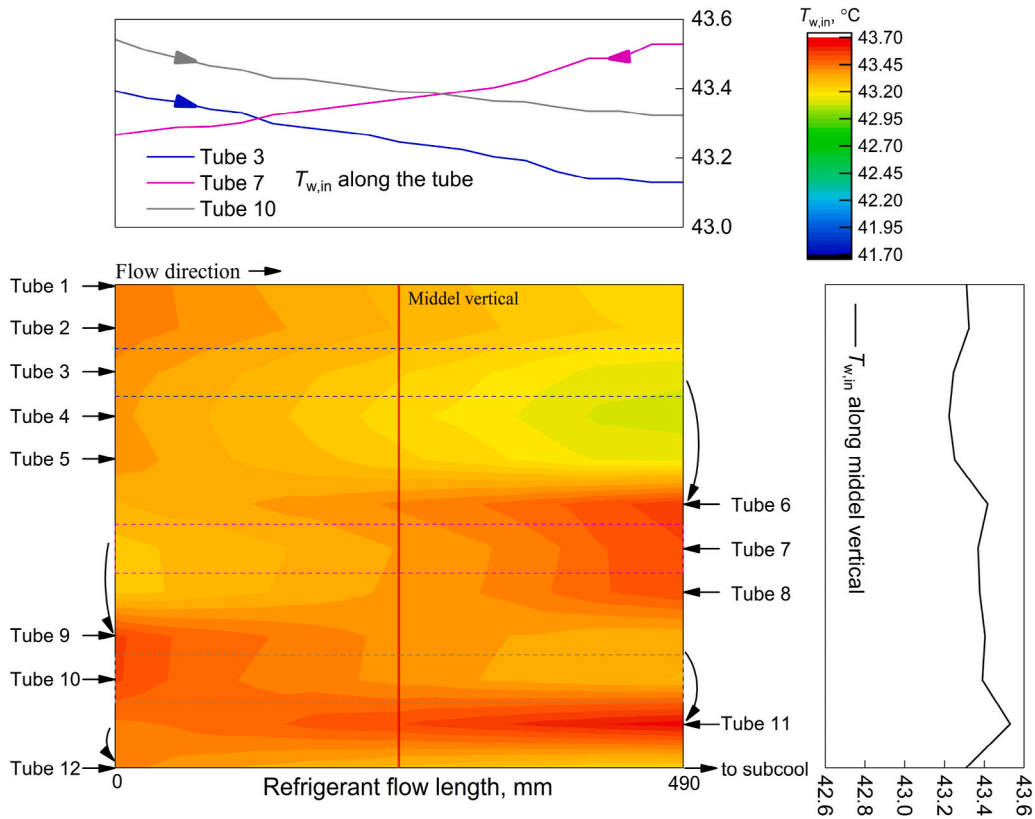


Fig. 8. Local  $T_w$  of the MPFC-LS

enhancement, especially at the entrance of parallel tubes. Take the comparison of Tube-pass 2 between the two condensers as an example, for the front half of tube-pass (0–245 mm in the x-axis) the averaged  $HTC$  is improved by 16.2 %, which is higher than that of 11.7 % for the rear half of tube-pass (245–450 mm in the x-axis). This trend is also demonstrated in the comparison of Figs. 6(b) and 7 (b), the slope of the local-averaged  $HTC$  varying with the flow path from 490 mm to 735 mm (the front half of the green line) is sharper than that from 735 mm to 980 mm (the rear half of the green line). Similar results can be found in Tube-passes 3–5 as well. When the refrigerant vapor quality is very high in tubes (by LS in mediate header), the two-phase flow pattern is mist flow and there is almost no liquid film sticking around the tube-wall but some droplets. The vapor with high velocity can interact with the tube-wall directly for condensation, thus the heat transfer coefficient is very high. When the condensation keeps developing and vapor quality decreases, the liquid film forms, becomes thick and, spreads around the tube-wall, which hampers the condensation of the refrigerant at the tube wall surface. Hence the heat transfer coefficient drops sharply in the tube along the flow direction. This can be called as entrance-effect of condensation heat transfer in tubes. Compared to the MPFC, one of the most unique features of MPFC-LS is to introduce and take advantage of this entrance effect by the liquid-vapor separation between adjacent tube-passes, and to maintain a high level of condensation heat transfer instead of single-phase heat transfer through the whole condenser. It is worth noticing that choosing an appropriate tube length and making fully use of this high heat transfer area is a key challenge for the design of MPFCs-LS.

Figs. 8 and 9 demonstrate the contour of the tube-wall temperature distribution for the MPFC-LS and MPFC. In general, the overall averaged  $T_w$  of MPFC-LS is 43.3 °C, 0.4 °C higher than that of 42.9 °C of MPFC. The temperature profiles of the single tube along the flow direction are also depicted in the figures on the top side of the two figures. These, as examples, are the results of tubes 7 and 10 (dash lines marked in the contour) and the mean  $T_w$  of the tubes of MPFC-LS are 0.18 °C and 0.25 °C higher than those of MPFC, respectively. Moreover, the temperature decreasing along the flow direction in MPFC-LS have the larger slope rate than MPFC because of the  $HTC$  decreasing sharply in the entrance-effect area. Based on the comparison of  $T_w$  profiles along the middle vertical cross-section between the two condensers (see Figs. 8 and 9), the raises of wall temperature in the downstream (Tube-passes 2–4) are higher than those in the upstream (Tube-pass 1). There is a distinct dropping (0.5 °C) of wall temperature for MPFC in the last tube (Tube 12) due to the low bulk temperature (large  $\Delta P$ ) and low  $HTC$  (low vapor quality). Notice that the highest  $T_w$  of MPFC-LS appears at the entrance of Tube-pass 4 (Tube 11) and the maximum increase of  $T_w$  (up to 0.63 °C) appears before but close to the exit of the condensers. In addition, the inlet air temperature is fixed and identical for these two condensers, so a higher tube-wall temperature corresponds to a larger mean temperature difference driving the heat transfer in the air side, which means a lower air velocity required to achieve a certain heat transfer rate, e.g. the fixed heat transfer rate 1300 W in present study.

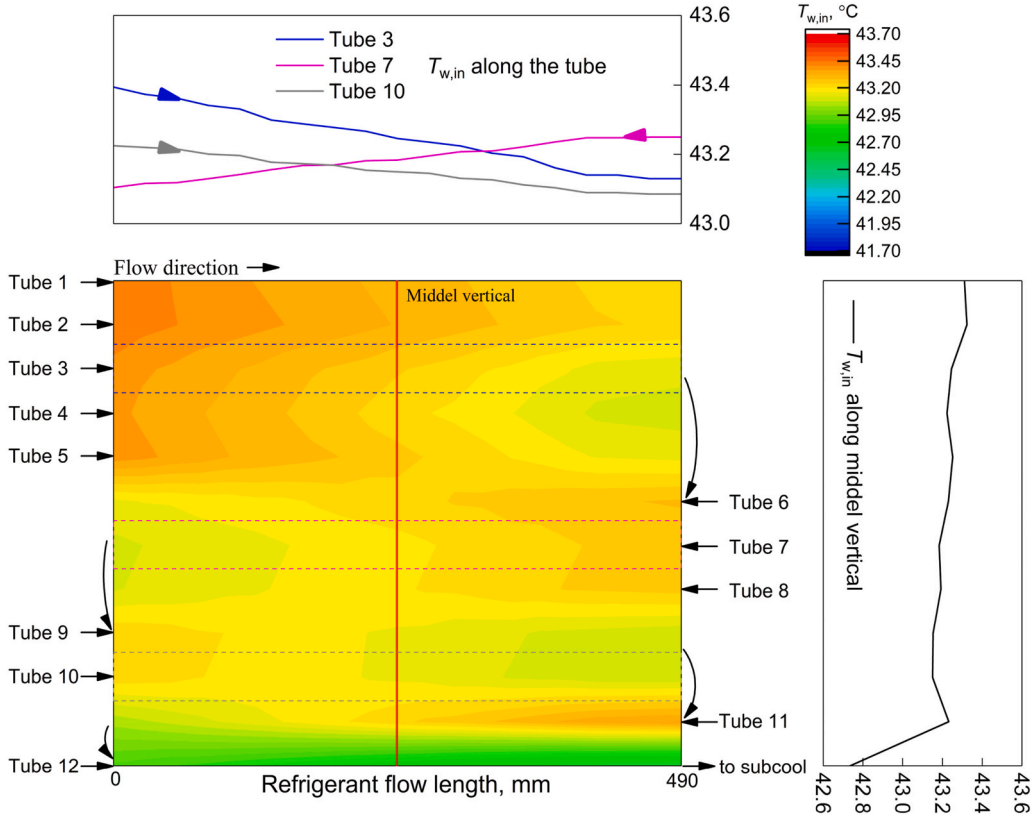


Fig. 9. Local  $T_w$  of the MPFC

### 3.3. Analysis based on the second law of thermodynamics

Entropy generation has been used to evaluate the performance of thermal devices especially where the phase-change process occurs [51]. In the present work, the heat transfer enhancement technique, i.e. liquid-vapor separation, is implemented to MPFC on the tube side, thus the analysis of entropy generation in this section focuses only on the refrigerant side. The entropy generated in a small segment is determined by Eq. (4):

$$d\dot{S}_{gen} = \frac{d\dot{q}}{T_w} + \dot{m}ds \tag{4}$$

$$d\dot{q} = -\dot{m}dh_r, \quad d\dot{q} = -\dot{m}dh_r \tag{5}$$

$$T_r ds = dh_r - v dP \tag{6}$$

Using the thermodynamic relations Eqs. (5) and (6), Eq. (4) can be written as:

$$d\dot{S}_{gen} = \frac{T_r - T_w}{T_r T_w} d\dot{q} - \frac{\dot{m}}{\rho T_r} dP \tag{7}$$

where  $T_r$  and  $T_w$  are the temperatures of the refrigerant and tube-wall, respectively.

In terms of exergy analysis, Hesselgeaves [52] indicated that the entropy generation rate was non-dimensionalised with the heat flow characteristic ( $Q/T_0$ ) in a condenser. Consequently, the entropy generation number, a non-dimensional measure of entropy generation, is defined by Eq. (8).

$$N_s = \frac{d\dot{S}_{gen} T_w}{d\dot{q}} \tag{8}$$

Substituting Eq. (7) into Eq. (8) yields:

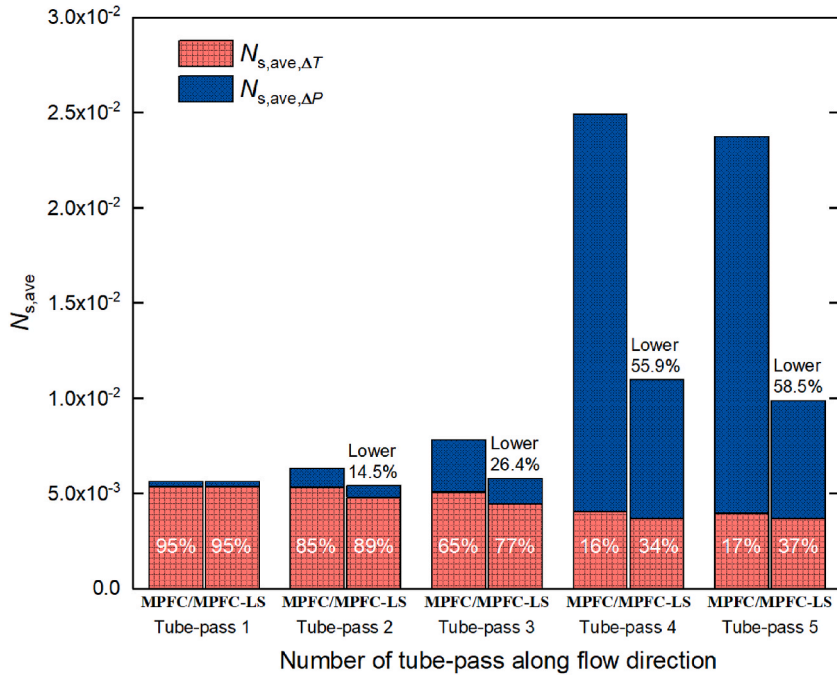


Fig. 10. Comparison of  $N_{s,ave}$  per tube-pass for condensers with and without LS.

$$N_s = \frac{T_r - T_w}{T_r} - \frac{\dot{m} \left( 1 - \frac{T_r - T_w}{T_r} \right)}{\rho} \frac{dP}{d\dot{q}} \tag{9}$$

Fig. 10 illustrates the comparison of the average entropy generation number,  $N_{s,ave}$ , corresponding to the parts due to temperature difference (red,  $N_{s,ave,\Delta T}$ ) and pressure drop (blue,  $N_{s,ave,\Delta P}$ ), as function of tube-pass number for MPFC and MPFC-LS. It can be seen from Eq. (9) that the large temperature difference,  $\Delta T$ , between the tube-wall and refrigerant increases the weight of first term on the right-hand side while the large pressure drop and mass flow rate as well as the low density increase the weight of the second term. As shown in Fig. 10, the downstream (Tube-passes 4 and 5) have larger  $N_{s,ave}$  than the upstream (Tube-passes 1–3) for both the

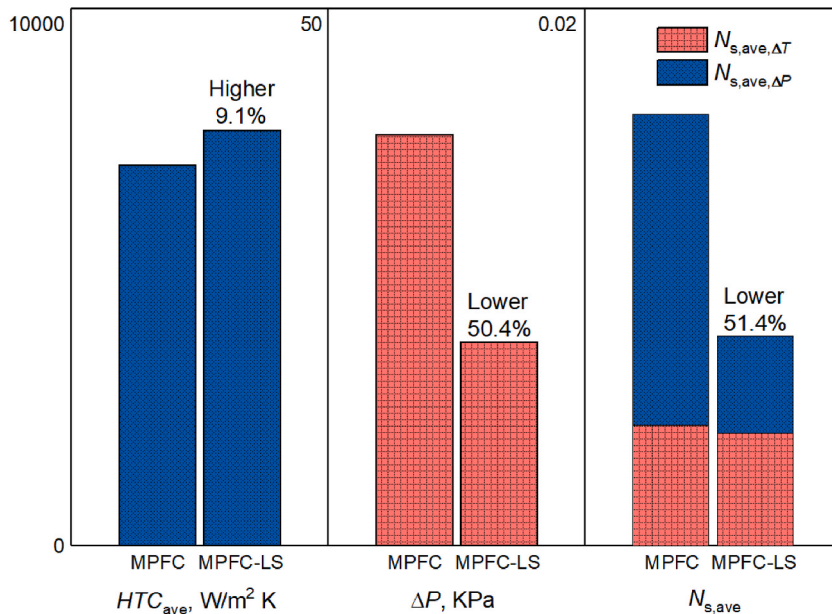


Fig. 11. Comparison of  $HTC_{ave}$ ,  $\Delta P$  and  $N_{s,ave}$  for condensers with and without LS.

condensers, due to the larger pressure drop and mass flux caused by the increased condensate that is not separated from the main stream. On the contrary, due to the lower pressure drop and mass flux (i.e. LS gets condensate filtered and keeps the vapor quality high in the tube),  $N_{s,ave}$  of any tube-pass of MPFC-LS is always lower than that of MPFC. This improvement is intensified significantly from 14.5 % to 58.5 % with the increase of the tube-pass number from two to five.

In addition, for both condensers, in the present simulations, the increasing  $HTC$  reduces the temperature difference between the tube-wall and refrigerant and then results in slightly decreasing  $N_{s,ave,\Delta T}$  along the flow direction. Due to the significant increase of  $N_{s,ave,\Delta P}$ , the percentages of the total  $N_{s,ave}$  from  $N_{s,ave,\Delta T}$  dramatically lower from 95 % in Tube-pass 1–17 % and 37 % in Tube-pass 5 for MPFC and MPFC-LS, respectively.

### 3.4. Comparison of overall performance of condensers with and without LS

In summary, using the given configurations and dimensions of the two condensers, as well as the pre-set simulation conditions, the comparison of overall performances between MPFC-LS and MPFC are demonstrated in Fig. 11. The results show that the average  $HTC$  on the refrigerant side of MPFC-LS is 7749 W/m<sup>2</sup> K, which is 9.1 % higher than that of 7102 W/m<sup>2</sup> K for MPFC. The total pressure drop of MPFC-LS is only 19.0 kPa, which is 50.4 % lower than that of 38.3 kPa for MPFC. In addition, the average entropy generation number,  $N_{s,ave}$ , of MPFC-LS is 51.4 % lower than that of MPFC. As seen in the figure, it can be found that the major contribution to the improvement of  $N_{s,ave}$  for MPFC-LS comes from the pressure drop (blue,  $N_{s,ave,\Delta P}$ ), which is reduced by almost 70.0 % compared with MPFC.

### 3.5. Optimization of tube-pass arrangement for condensers with liquid-vapor separation

The primary strategy for the arrangement of tube passes is the alteration in the number of passes. To optimize the tube pass configuration for the MPFC-LS, this work elevated 19 different tube pass arrangement schemes, as detailed in Table 6. The simulation conditions used in this section are listed in Table 7. Through preliminary calculations, it was determined that the first 20 tubes, which encompass the entire heat transfer region of the condenser (including superheating, condensation, and subcooling), would be fitted with headers. The last four tubes were designated for the subcooling section of the condenser. The guideline for setting the number of tubes per pass was that the downstream passes should contain fewer tubes than the adjacent upstream pass, in line with the direction of refrigerant flow. To highlight the enhanced performance of the MPFC-LS, a serpentine condenser was chosen as a baseline configuration. This baseline consists of 24 tubes connected by U-shaped bends without headers and liquid-vapor separation. Table 6 lists the numbering of each tube pass configuration for subsequent discussion and analysis, with NP indicating the number of tube passes in the condenser. For example, in configuration ID 3, NP is 8, indicating that the 20 tubes are divided into 8 passes, with the tube pass arrangement being (6-4-3-3-1-1-1-1). The reduction in the number of tubes per pass along the flow direction is based on the theory of liquid-vapor separation during condensation, where the refrigerant mass flow rate decreases as condensation and liquid-vapor separation continuously are implemented. To maintain uniform heat transfer across the entire condenser, the number of tubes in the next pass is reduced to increase the mass flow rate per tube. Moreover, based on the theory of condensation heat transfer, when the flow velocity inside the tubes is too low, even at high vapor quality, the refrigerant is likely to be in a stratified or wavy flow regime, where the condensation heat transfer coefficient is relatively low. Hence, the number of tubes in the first pass is maximized to 6.

The comprehensive evaluation index used for optimizing the MPFC-LS tube passes was based on the overall efficiency of the condenser  $\eta$ , as proposed by Wang et al. [53] in their study on MPFCs. This index evaluates the condenser's overall performance, considering both the heat transfer performance and pressure drop under different structural and operational conditions.  $\eta$  can be

**Table 6**  
Schemes of tube-pass arrangement for MPFCs-LS

ID	Number of tube passes (NP)	Tube-pass arrangement	Number of tubes in the first pass	Number of subcooling tubes
1	8	4-4-4-1-1-1-1-1	4	4
2	8	5-4-4-3-1-1-1-1	5	4
3	8	6-4-3-3-1-1-1-1	6	4
4	9	4-4-3-3-2-1-1-1-1	4	4
5	9	5-4-3-3-1-1-1-1-1	5	4
6	9	6-4-3-2-1-1-1-1-1	6	4
7	10	3-3-3-3-2-2-1-1-1-1	3	4
8	10	4-3-3-3-2-1-1-1-1-1	4	4
9	10	5-4-2-2-2-1-1-1-1	5	4
10	10	6-4-2-2-1-1-1-1-1-1	6	4
11	11	3-3-2-2-2-2-2-1-1-1-1	3	4
12	11	4-3-2-2-2-2-1-1-1-1-1	4	4
13	11	5-3-2-2-2-1-1-1-1-1-1	5	4
14	11	6-3-2-2-1-1-1-1-1-1-1	6	4
15	12	2-2-2-2-2-2-2-2-1-1-1-1	2	4
16	12	3-2-2-2-2-2-2-1-1-1-1-1	3	4
17	12	4-2-2-2-2-2-1-1-1-1-1-1	4	4
18	12	5-2-2-2-2-1-1-1-1-1-1-1	5	4
19	12	6-2-2-2-1-1-1-1-1-1-1-1	6	4

**Table 7**  
Simulation conditions of the condensers for optimizing tube-pass arrangement

Parameter	$m_{r,in}$ (kg s <sup>-1</sup> )	$P_{r,in}$ (kPa)	$T_{r,in}$ (°C)	$T_{a,in}$ (°C)
Value	0.0232	1900	82.00	35.00

calculated by:

$$\eta = \frac{Q}{\Delta P_r \cdot M_r / \rho_{r,mean} + \Delta P_a G_a} \tag{10}$$

where  $Q$  is the heat transfer rate of the condenser,  $\rho_{r,mean}$  denotes the average refrigerant density between the inlet and outlet,  $\Delta P_r$  and  $M_r$  represent the refrigerant-side pressure drop and mass flow rate, respectively, while  $\Delta P_a$  and  $G_a$  represent the air-side pressure drop and volumetric flow rate, respectively.

Figs. 12–14 present the comparisons of the overall efficiency of the condenser, heat transfer rate, and pressure drop of the MPFCs-LS with different tube pass arrangements. The x-axis corresponds to the condenser ID in Table 6 while the y-axis represents the ratio of the performance parameters of the MPFC-LS to those of the baseline serpentine condenser. Values greater than 1 indicate that the respective performance parameter of the MPFC-LS is superior to that of the serpentine condenser, while values less than 1 indicate inferior performance. The black lines with symbols in the figures categorize the MPFC-LS configurations into five regions based on the number of tube passes. The configurations within each region share the same number of tube passes and are arranged in increasing order of the number of tubes in the first pass. As NP increases, all performance parameters exhibit a parabolic trend within the calculated operating range, showing relative extrema.

The overall efficiency and heat transfer rate of the MPFC-LS follow a convex parabolic trend, first increasing and then decreasing, while the pressure drop follows a concave parabolic trend, first decreasing and then increasing. The observed maxima and minima align with the basic selection criteria for MPFC-LS:  $\eta$  and  $Q$  should be as large as possible, while  $\Delta P$  should be minimized.

Given that the evaluated condensers in this section are with liquid-vapor separation, with the refrigerant entering each tube pass at an idealized vapor quality of 1.0, the observed changes in performance parameters are solely due to the distribution of refrigerant mass flow across the entire MPFC-LS. Generally, an increase in the number of tube passes results in a higher number of single-tube passes downstream, which increases the refrigerant pressure drop across the entire MPFC-LS, while simultaneously enhancing the heat transfer rate and overall efficiency. Adjusting the number of tubes in the first pass while keeping the number of passes constant can amplify or mitigate these effects. This explains why, within a region with a constant number of passes, the performance parameters of the MPFCs-LS exhibit a trend similar to that observed with changes in the number of passes.

It is noteworthy that, as shown in Fig. 12, the overall efficiency trend of the MPFCs-LS is primarily driven by the change in heat transfer rate, while being secondarily influenced by the pressure drop. The heat transfer rate remains high even after reaching its maximum value for configurations with more passes and fewer tubes in the first pass. However, the continuous increase in pressure drop after its minimum value causes a significant decrease in overall efficiency after it reaches its peak. Considering all factors, the MPFC-LS configuration with a tube pass arrangement of 3-3-2-2-2-2-2-1-1-1-1 demonstrated the best comprehensive performance among the evaluated schemes listed in Table 6. Moreover, compared to the baseline serpentine condenser, all MPFC-LS configurations, regardless of the tube pass arrangement, achieved a substantial reduction in pressure drop by 84 %–98 % while experiencing only a slight decrease in heat transfer rate of approximately 1 %–5 %. Overall, the MPFC-LS configurations outperformed the baseline in terms of overall efficiency by 5 %–9 % within the calculated range.

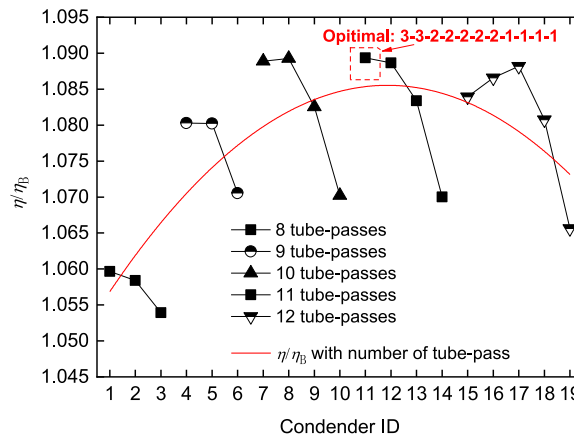


Fig. 12. Whole performance comparisons of MPFC-LS with different tube-pass arrangements.

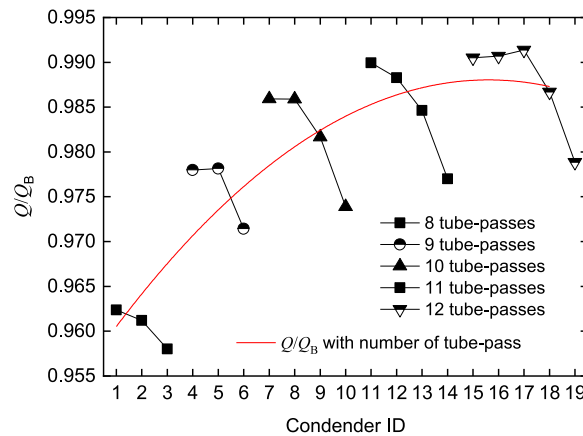


Fig. 13. Heat transfer rate comparisons of MPFC-LS with different tube-pass arrangements.

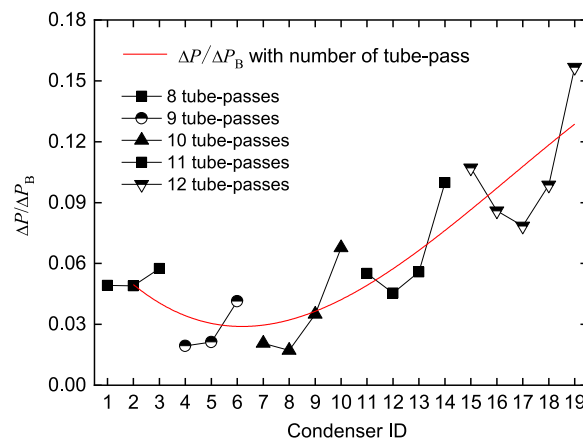


Fig. 14. Pressure drop comparisons of MPFC-LS with different tube-pass arrangements.

#### 4. Conclusions

Numerical simulations have been performed to investigate into the mechanisms of liquid-vapor separation to enhance condensation heat transfer. The local and averaged heat transfer and pressure drop are compared for multi-pass parallel flow condensers with and without liquid-vapor separation (MPFC and MPFC-LS). The entropy analysis has also been performed to examine the contributions of entropy generation in tubes by heat transfer and pressure drop. Finally, the tube pass arrangement of the MPFC-LS has been optimized.

Due to the liquid-vapor separation, the refrigerant mass fluxes in tubes of Tube-passes 2–5 of MPFC-LS are lower compared with their previously adjacent Tube-pass while the averaged vapor qualities in tubes of Tube-passes 2–5 remain high.

Compared with MPFC, the tube-wall temperatures of MPFC-LS are generally higher especially in the downstream and the maximum difference in tube-wall temperature appears near the exit of the condensers.

For MPFC-LS, the averaged heat-transfer coefficient in tubes increases slightly from 13.8 % to 17.8 % due to the LS, the pressure drop and the average entropy generation number in tubes decrease significantly from 23.4 % to 58.7 % and from 14.5 % to 58.5 %, respectively.

The overall averaged heat-transfer coefficient of MPFC-LS is 9.1 % higher, and the overall pressure drop and the overall averaged entropy generation number are 50.4 % and 51.4 % lower compared to MPFC, respectively.

The number of tube passes and the number of tubes in the first pass significantly influence the heat transfer performance of MPFCs-LS. Among the evaluated configurations, the MPFC-LS with a tube pass arrangement of 3-3-2-2-2-2-2-1-1-1-1 exhibited the best overall performance. Compared to the baseline serpentine condenser, all MPFC-LS configurations achieved a significant reduction in pressure drop by 84 %–98 % and improved overall efficiency by 5 %–9 %, with almost the same capacity in heat transfer.

## CRediT authorship contribution statement

**Jin Huan Pu:** Writing – original draft, Software, Investigation, Formal analysis. **Nan Hua:** Writing – original draft, Software, Investigation, Formal analysis, Conceptualization. **Xiaodong Jian:** Investigation, Formal analysis, Conceptualization. **Ying Chen:** Investigation, Formal analysis, Conceptualization. **Yongliang Li:** Investigation, Formal analysis. **Tong Yang:** Formal analysis, Conceptualization. **Hua Sheng Wang:** Writing – review & editing, Investigation, Formal analysis, Conceptualization.

## Declaration of competing interest

The authors declare that they have no known competing financial interests or personal relationships that could have appeared to influence the work reported in this paper.

## Acknowledgement

The authors gratefully acknowledge the financial support from the Shandong Provincial Natural Science Foundation (ZR2023QE262), and the Engineering and Physical Sciences Research Council of the UK (EP/N020472/1) and (EP/T022701/1). The scientific calculations in this paper have been done on the HPC Cloud Platform of Shandong University.

## Data availability

Data will be made available on request.

## References

- [1] H.S. Wang, J.W. Rose, Film condensation in horizontal microchannels: effect of channel shape, *Int. J. Therm. Sci.* 45 (12) (2006) 1205–1212, <https://doi.org/10.1016/j.ijthermalsci.2006.03.004>.
- [2] H.S. Wang, J.W. Rose, Theory of heat transfer during condensation in micro-channels, *Int. J. Heat Mass Tran.* 54 (11–12) (2011) 2525–2534, <https://doi.org/10.1016/j.ijheatmasstransfer.2011.02.009>.
- [3] H.S. Wang, J.W. Rose, Heat transfer and pressure drop during laminar annular flow condensation in micro-channels, *Exp. Heat Transf.* 26 (2–3) (2013) 247–265, <https://doi.org/10.1080/08916152.2012.737261>.
- [4] H.S. Wang, H. Honda, Condensation of refrigerants in horizontal microfin tubes: comparison of prediction methods for heat transfer, *Int. J. Refrig.* 26 (4) (2003) 452–460, [https://doi.org/10.1016/S0140-7007\(02\)00158-5](https://doi.org/10.1016/S0140-7007(02)00158-5).
- [5] A.S. Dalkilic, S. Wongwises, Intensive literature review of condensation inside smooth and enhanced tubes, *Int. J. Heat Mass Tran.* 52 (15–16) (2009) 3409–3426, <https://doi.org/10.1016/j.ijheatmasstransfer.2009.01.011>.
- [6] K.N. Agrawal, A. Kumar, M.A. Behabadi, H.K. Varma, Heat transfer augmentation by coiled wire inserts during forced convection condensation of R-22 inside horizontal tubes, *Int. J. Multiphas. Flow* 24 (4) (1998) 635–650, [https://doi.org/10.1016/S0301-9322\(97\)00061-X](https://doi.org/10.1016/S0301-9322(97)00061-X).
- [7] T. Ji, L. Liebenberg, J.P. Meyer, Heat transfer enhancement during condensation in smooth tubes with helical wire inserts, *Heat Transf. Eng.* 30 (5) (2009) 337–352, <https://doi.org/10.1080/01457630802414466>.
- [8] K. Oh, S. Lee, T. Park, Y. Kim, Multistage gas and liquid phase separation condenser, US Patent No. 0217567 (2003).
- [9] X. Peng, D. Wu, G. Lu, Z. Wang, M. Huang, Liquid-Vapor Separation Air Condenser, vol. 4, 2006. China Patent No. 200610113304.
- [10] K. Huang, J. Li, J. Chen, Y. Chen, X. Luo, Y. Liang, J. He, Z. Yang, Explorations of multi-pass-orifice header in the liquid-separation condenser by using CFD simulation, *Int. J. Heat Mass Tran.* 200 (2023) 123482, <https://doi.org/10.1016/j.ijheatmasstransfer.2022.123482>.
- [11] K. Oh, S. Lee, T. Park, Y. Kim, Multistage gas and liquid phase separation condenser, U.S. Patent 6 (769) (2004-8-3) 269.
- [12] J. Li, P. Hrnjak, Improvement of condenser performance by phase separation confirmed experimentally and by modelling, *Int. J. Refrig.* 78 (2017) 60–69, <https://doi.org/10.1016/j.ijrefrig.2017.03.018>.
- [13] J. Li, P. Hrnjak, Separation in condensers as a way to improve efficiency, *Int. J. Refrig.* 79 (2017) 1–9, <https://doi.org/10.1016/j.ijrefrig.2017.03.017>.
- [14] J. Li, P. Hrnjak, Visualization and quantification of separation of liquid-vapor two-phase flow in a vertical header at low inlet quality, *Int. J. Refrig.* 85 (2018) 144–156, <https://doi.org/10.1016/j.ijrefrig.2017.09.018>.
- [15] J. Li, P. Hrnjak, Numerical simulation of two-phase flow in the second header of MAC condenser, SAE Technical Paper (2019), <https://doi.org/10.4271/2019-01-1065>.
- [16] L. Ye, M.W. Tong, X. Zeng, Design and analysis of multiple parallel-pass condensers, *Int. J. Refrig.* 32 (6) (2009) 1153–1161, <https://doi.org/10.1016/j.ijrefrig.2009.01.012>.
- [17] L. Jia, A Upright Vertical Type Condenser and Heat Transfer Method, 201410743731.5, PRC Patent, 2014.
- [18] X. Zhang, L. Jia, C. Dang, Q. Peng, Visualization investigation on flowing condensation in horizontal small channels with liquid separator, *J. Therm. Sci.* 27 (1) (2018) 48–54, <https://doi.org/10.1007/s11630-018-0983-6>.
- [19] X. Zhang, L. Jia, Q. Peng, C. Dang, Experimental study of condensation heat transfer in a condenser with a liquid-vapor separator, *Appl. Therm. Eng.* 152 (2019) 196–203, <https://doi.org/10.1016/j.applthermaleng.2019.02.086>.
- [20] D. Wu, Z. Wang, G. Lu, X.F. Peng, High-performance air cooling condenser with liquid-vapor separation, *Heat Transf. Eng.* 31 (12) (2010) 973–980, <https://doi.org/10.1080/01457631003638952>.
- [21] Y. Chen, N. Hua, L.S. Deng, Performances of a split-type air conditioner employing a condenser with liquid-vapor separation baffles, *Int. J. Refrig.* 35 (2) (2012) 278–289, <https://doi.org/10.1016/j.ijrefrig.2011.10.014>.
- [22] N. Hua, Y. Chen, E. Chen, L. Deng, W. Zheng, Z. Yang, Prediction and verification of the thermodynamic performance of vapor-liquid separation condenser, *Energy* 58 (2013) 384–397, <https://doi.org/10.1016/j.energy.2013.05.034>.
- [23] N. Hua, H. Xi, R.J. Xu, Y. Chen, H.S. Wang, Numerical simulation of multi-pass parallel flow condensers with liquid-vapor separation, *Int. J. Heat Mass Tran.* 142 (2019) 118469, <https://doi.org/10.1016/j.ijheatmasstransfer.2019.118469>.
- [24] T. Zhong, Y. Chen, N. Hua, W. Zheng, X. Luo, S. Mo, In-tube performance evaluation of an air-cooled condenser with liquid-vapor separator, *Appl. Energy* 136 (2014) 968–978, <https://doi.org/10.1016/j.apenergy.2014.07.032>.
- [25] S. Mo, X. Chen, Y. Chen, Z. Yang, Passive control of gas-liquid flow in a separator unit using an apertured baffle in a parallel-flow condenser, *Exp. Therm. Fluid Sci.* 53 (2014) 127–135, <https://doi.org/10.1016/j.expthermflusci.2013.11.017>.
- [26] T. Zhong, Y. Chen, W. Zheng, N. Hua, X. Luo, Experimental investigation on microchannel condensers with and without liquid-vapor separation headers, *Appl. Therm. Eng.* 73 (2) (2014) 1510–1518, <https://doi.org/10.1016/j.applthermaleng.2014.08.047>.

- [27] T. Zhong, Y. Chen, Q. Yang, S. Mo, X. Luo, J. Xu, Experimental investigation on the thermodynamic performance of double-row liquid–vapor separation micro-channel condenser, *Int. J. Refrig.* 67 (2016) 373–382, <https://doi.org/10.1016/j.ijrefrig.2016.02.020>.
- [28] Y. Chen, N. Hua, D. Wu, A comparative study of fin-and-tube heat exchangers with and without liquid-vapor separation in air conditioning units, *Int. J. Green Energy* 11 (5) (2014) 488–499, <https://doi.org/10.1080/15435075.2013.770396>.
- [29] T. Zhong, L. Ding, S. Chen, Y. Chen, Q. Yang, Y. Luo, Effect of a double-row liquid–vapor separation condenser on an air-conditioning unit performance, *Appl. Therm. Eng.* 142 (2018) 476–482, <https://doi.org/10.1016/j.applthermaleng.2018.07.015>.
- [30] J. Chen, Y. Li, R. Ding, X. Lin, Y. Chen, Y. Luo, Z. Yang, Comparative performance of air-conditioning systems with different refrigerant circuitries in liquid-separation condenser, *Int. J. Refrig.* 92 (2018) 154–164, <https://doi.org/10.1080/15435075.2013.770396>.
- [31] J. Chen, R. Ding, Y. Li, X. Lin, Y. Chen, Y. Luo, Z. Yang, Application of a vapor–liquid separation heat exchanger to the air conditioning system at cooling and heating modes, *Int. J. Refrig.* 100 (2019) 27–36, <https://doi.org/10.1016/j.ijrefrig.2018.10.030>.
- [32] J. Chen, L. Chen, X. Lin, Y. Chen, X. Luo, Z. Yang, Y. Liang, Performance of heat pump water heater (HPWH) with and without liquid-separation: detailed experimental comparisons, *Appl. Therm. Eng.* 179 (2020) 115713, <https://doi.org/10.1016/j.applthermaleng.2020.115713>.
- [33] J. Chen, L. Chen, J. Li, Y. Chen, X. Luo, Y. Liang, Z. Yang, J. He, Potentials of implementing liquid-separation to a transient wrap-around microchannel condenser coil within heat pump water heater, *Energy* 254 (2022) 124261, <https://doi.org/10.1016/j.energy.2022.124261>.
- [34] J. Chen, N. Yang, J. Li, J. He, Y. Chen, X. Luo, Y. Liang, Evaluations of heat pump water heater with liquid-separation condensation from perspectives of performance enhancement and heat exchange area reduction, *Int. J. Refrig.* 161 (2024) 21–30, <https://doi.org/10.1016/j.ijrefrig.2024.02.026>.
- [35] X. Luo, Z. Yi, B. Zhang, S. Mo, C. Wang, M. Song, Y. Chen, Mathematical modelling and optimization of the liquid separation condenser used in organic rankine cycle, *Appl. Energy* 185 (2017) 1309–1323, <https://doi.org/10.1016/j.apenergy.2015.12.073>.
- [36] X. Luo, G. Qiu, J. Qi, J. Chen, C. Wang, Z. Yang, Y. Chen, Mathematical modelling and structural optimization of a micro-channel liquid separation condenser in organic rankine cycle and refrigeration cycle, *Appl. Therm. Eng.* 152 (2019) 231–246, <https://doi.org/10.1016/j.applthermaleng.2019.02.050>.
- [37] Z. Yi, X. Luo, J. Chen, Y. Chen, Mathematical modelling and optimization of a liquid separation condenser-based organic rankine cycle used in waste heat utilization, *Energy* 139 (2017) 916–934, <https://doi.org/10.1016/j.energy.2017.08.060>.
- [38] X. Luo, Z. Yi, Z. Chen, Y. Chen, S. Mo, Performance comparison of the liquid–vapor separation, parallel flow, and serpentine condensers in the organic rankine cycle, *Appl. Therm. Eng.* 94 (2016) 435–448, <https://doi.org/10.1016/j.applthermaleng.2015.10.074>.
- [39] J.H. Pu, N. Hua, Y. Chen, Y. Li, T. Yang, H.S. Wang, Modelling and numerical simulation of heat transfer and hydrodynamic performance of multi-pass parallel flow condensers—A novel algebraic method to determine flow distribution, *Int. Commun. Heat Mass Transf.* 159 (2024) 107941, <https://doi.org/10.1016/j.icheatmasstransfer.2024.107941>.
- [40] J. Yu, S. Koyama, Condensation heat transfer of pure refrigerants in microfin tubes, in: *Proc. Int. Refrigeration Conference at Purdue University, West Lafayette, USA, 1998*, pp. 325–330.
- [41] A. Cavallini, D. Del Col, S. Mancini, L. Rossetto, Condensation of pure and near-azeotropic refrigerants in microfin tubes: a new computational procedure, *Int. J. Refrig.* 32 (1) (2009) 162–174, <https://doi.org/10.1016/j.ijrefrig.2008.08.004>.
- [42] N.H. Kim, Condensation heat transfer and pressure drop of R-410A in a 7.0 mm OD microfin tube at low mass fluxes, *Heat Mass Transf.* 52 (12) (2016) 2833–2847, <https://doi.org/10.1017/s00231-016-1789-2>.
- [43] Z. Wu, B. Sundén, V.V. Wadekar, W. Li, Heat transfer correlations for single phase flow, condensation, and boiling in microfin tubes, *Heat Transfer Eng.* 36 (6) (2015) 582–595, <https://doi.org/10.1080/01457632.2014.939531>.
- [44] C.C. Wang, W.S. Lee, W.J. Sheu, A comparative study of compact enhanced fin-and-tube heat exchangers, *Int. J. Heat Mass Tran.* 44 (18) (2001) 3565–3573, [https://doi.org/10.1016/S0017-9310\(01\)00011-4](https://doi.org/10.1016/S0017-9310(01)00011-4).
- [45] H. Haraguchi, Studies on condensation of HCFC-22, HFC-134a and HCFC-123 in horizontal tubes, kyushu university, Dr. Eng. Thesis (1994) [in Japanese].
- [46] S. Nozu, H. Katayama, H. Nakata, H. Honda, Condensation of a refrigerant CFC11 in horizontal microfin tubes, *Exp. Therm. Fluid Sci.* 18 (1998) 82–96, [https://doi.org/10.1016/S0894-1777\(98\)00010-7](https://doi.org/10.1016/S0894-1777(98)00010-7).
- [47] J.G. Collier, J.R. Thome, Convective Boiling and Condensation, 3rd, Oxford University Press, New York, 1994.
- [48] J.R. Thome, Engineering Databook III, Wolverine Tube, Inc, Huntsville, AL, USA, 2004.
- [49] J.M. Yin, C.W. Bullard, P.S. Hrnjak, Single-phase pressure drop measurements in a microchannel heat exchanger, *Heat Transfer Eng.* 23 (4) (2002) 3–12, <https://doi.org/10.1080/01457630290090455>.
- [50] L. Liebenberg, J.P. Meyer, A review of flow pattern-based predictive correlations during refrigerant condensation in horizontally smooth and enhanced tubes, *Heat Transfer Eng.* 29 (1) (2008) 3–19, <https://doi.org/10.1080/01457630701677049>.
- [51] A. Bejan, *Entropy Generation Through Heat and Fluid Flow*, Wiley, New York, 1982.
- [52] J.E. Hesselgreaves, Rationalisation of second law analysis of heat exchangers, *Int. J. Heat Mass Tran.* 43 (22) (2000) 4189–4204, [https://doi.org/10.1016/S0017-9310\(99\)00364-6](https://doi.org/10.1016/S0017-9310(99)00364-6).
- [53] T. Wang, B. Gu, B. Wu, H. Ma, C. Qian, Modeling for multi-pass parallel flow condenser with the effect of refrigerant mal-distribution, *Int. J. Refrig.* 60 (2015) 234–246, <https://doi.org/10.1016/j.ijrefrig.2015.08.015>.